3D-QSAR and Molecular Docking Studies on Benzotriazoles

Bull. Korean Chem. Soc. **2013**, Vol. 34, No. 8   2387

3D-QSAR and Molecular Docking Studies on Benzotriazoles as Antiproliferative Agents and Histone Deacetylase Inhibitors

Xiaolin Li,[†] Jie Fu,[†,‡,*] Wei Shi,[†] Yin Luo,[‡] Xiaowei Zhang,[†] Hailiang Zhu,[‡] and Hongxia Yu[†,*]

[†]*State Key Laboratory of Pollution Control and Resource Reuse, School of the Environment, Nanjing University, Nanjing 210023, P.R. China. *E-mail: hongxiayu01@yahoo.com.cn*
[‡]*State Key Laboratory of Pharmaceutical Biotechnology, School of Life Sciences, Nanjing University, Nanjing 210093, P.R. China. *E-mail: jiejeff8@gmail.com*

Benzotriazole is an important synthetic auxiliary for potential clinical applications. A series of benzotriazoles as potential antiproliferative agents by inhibiting histone deacetylase (HDAC) were recently reported. Three-dimensional quantitative structure-activity relationship (3D-QSAR), including comparative molecular field analysis (CoMFA) and comparative molecular similarity indices analysis (CoMSIA), were performed to elucidate the 3D structural features required for the antiproliferative activity. The results of both ligand-based CoMFA model ($q^2 = 0.647$, $r^2 = 0.968$, $r^2_{pred} = 0.687$) and CoMSIA model ($q^2 = 0.685$, $r^2 = 0.928$, $r^2_{pred} = 0.555$) demonstrated the highly statistical significance and good predictive ability. The results generated from CoMFA and CoMSIA provided important information about the structural characteristics influence inhibitory potency. In addition, docking analysis was applied to clarify the binding modes between the ligands and the receptor HDAC. The information obtained from this study could provide some instructions for the further development of potent antiproliferative agents and HDAC inhibitors.

Key Words : Antiproliferative, Benzotriazole, 3D-QSAR, Molecular docking

Introduction

Cancer is a leading cause of death throughout the world.[1] Recently, many classes of compounds showed antiproliferative activity against human cancer cells including dihydro-1,3,5-triazines,[2] bis-quinolinium derivatives,[3] 4-aminomethylidene derivatives,[4] aroylacrylic acids,[5] *etc.* were synthesized and several compounds showed promising inhibitory potency in clinical trials. However, the traditional drug discovery only by chemical synthesis remains a labor intensive, time-consuming and expensive task for researchers. To facilitate the drug design process, computer-aided drug design (CADD) approach as a productive and cost-effective technology should be used in combination with experimental practices.[6] The addition of CADD to the drug discovery could lead to a reduction of over 50% in the cost of drug design[7]. Quantitative structure-activity relationship (QSAR), especially three-dimensional QSAR (3D-QSAR) including comparative molecular field analysis (CoMFA) and comparative molecular similarity indices analysis (CoMSIA), is a powerful CADD approach that has been widely employed in drug discovery to minimize the time and cost of experimental evaluations.[8,9] Furthermore, molecular docking, which are beneficial to improve our knowledge about the protein-ligand interactions at the atomic level, have become an integral part of many structure-based computational simulations of compounds and are also utilized in current drug design process.[10,11] The *in silico* study combining structure-based 3D-QSAR and molecular docking have emerged as a useful tool to predict the biological activities of compounds and present a comprehensive feature for the ligand-receptor interactions.[12-14]

Benzotriazole is an important synthetic auxiliary with versatile applications in organic chemistry. Benzotriazole derivatives have attracted great attention because of their diverse biological activities and potential clinical applications, especially their ability to induce growth inhibition in cancer cells.[15,16] The design and synthesis of benzotriazoles as anticancer drugs have been widely reported.[17,18] Recently, a series of benzotriazoles were synthesized and their antiproliferative activities against human cancer cells were reported.[19] Some of the benzotriazoles showed considerable activity with the half maximal inhibitory concentration (IC_{50}) values being 1.2-2.4 nM. Further investigation indicated the antiprolierative functions of these benzotriazoles were possibly associated with their significant histone deacetylase (HDAC) inhibitory activities. HDAC, predominantly in histones H3 and H4, catalyzes the deacetylation of lysine (Lys) resides, and abnormal recruitment of HDACs has been clearly linked to carcinogenesis.[20,21]

In the present paper, *in silico* studies of these benzotriazoles were carried out by using structure-based QSAR and molecular docking approaches. 3D-QSAR including CoMFA and CoMSIA were performed to predict the antiproliferative activities of these compounds and depict the key structural elements that might affect the inhibitory activity. The robustness and predictive ability were validated statistically by several internal and external validation strategies. Meanwhile, molecular docking was employed to determine the binding modes of two ligands with much different activities to the
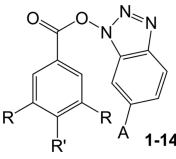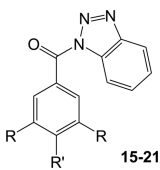
catalytic core of an archaebacterial HDAC homolog (histone deacetylase-like protein, HDLP). The objectives of this article are (1) to offer more insight into understanding the structure-activity relationship of these benzotriazoles; (2) to elucidate how their chemical structures influence the inhibitory activity; and (3) to disclose the detailed interaction mechanisms of these benzotriazoles with HDLP.

Experimental

Data Set. The structures and the antiproliferative activities of 21 benzotriazoles were taken from the previous literature.[19] The antiproliferative activity against one kind of human cancer cell, oral epidermoid carcinoma KB cell, was tested taking doxorubicin as the positive control. The antiproliferative activity in terms of IC_{50} (nM) was calculated and converted to the corresponding pIC_{50} (-log IC_{50}) and used as dependent variable in CoMFA and CoMSIA model. The whole data set was divided into training set (containing 17 compounds) for 3D-QSAR model generation and test set (containing 4 compounds) for model validation, respectively. Their structures and activity values are displayed in Tables 1 and 2.

The 3D-structures of benzotriazoles were initially built in Sybyl 7.3 molecular modeling package (Tripos Inc, St. Louis, MO, USA). Structural energy minimization was performed using Powell gradient algorithm and the Tripos force field[22] with a convergence criterion of 0.001 kcal/mol·Å and a maximum of 1000 iterations. Partial atomic charges were

Table 1. Structures of the selected compounds

Structure	Compound	Substituent		
		R	R'	A
	1	H	H	H
	2[a]	H	OH	H
	3	OH	H	H
	4	OH	OH	H
	5	H	OCH₃	H
	6	OCH₃	H	H
	7	OCH₃	OCH₃	H
1-14	**8**[a]	H	H	OCH₃
	9	H	OH	OCH₃
	10	OH	H	OCH₃
	11	OH	OH	OCH₃
	12	H	OCH₃	OCH₃
	13[a]	OCH₃	H	OCH₃
	14	OCH₃	OCH₃	OCH₃
		R	R'	
	15	H	H	
	16	H	OH	
	17[a]	OH	H	
15-21	**18**	OH	OH	
	19	H	OCH₃	
	20	OCH₃	H	
	21	OCH₃	OCH₃	

[a]Compounds in the test set.

Table 2. Observed and predicted pIC_{50} of the selected compounds

| Compound	Obs. pIC_{50}	CoMFA		CoMSIA	
		Pred.	Resid.	Pred.	Resid.
1	-2.02	-1.94	-0.08	-2.06	0.04
2[a]	-1.94	-1.83	-0.11	-1.68	-0.26
3	-1.85	-1.69	-0.16	-1.85	0
4	-1.26	-1.39	0.13	-1.27	0.01
5	-1.63	-1.38	-0.25	-1.69	0.06
6	-1.57	-1.40	-0.17	-1.07	-0.50
7	-0.08	-0.24	0.16	-0.15	0.07
8[a]	-2.32	-2.50	0.18	-2.51	0.19
9	-2.17	-2.28	0.11	-1.99	-0.18
10	-2.18	-2.25	0.07	-2.34	0.16
11	-1.91	-2.02	0.11	-1.85	-0.06
12	-1.99	-2.04	0.05	-2.13	0.14
13[a]	-1.54	-1.94	0.40	-1.58	0.04
14	-1.04	-0.93	-0.11	-0.90	-0.14
15	-2.82	-2.77	-0.05	-2.81	-0.01
16	-2.76	-2.71	-0.05	-2.78	0.02
17[a]	-2.76	-2.63	-0.13	-2.62	-0.14
18	-2.59	-2.56	-0.03	-2.57	-0.02
19	-2.70	-2.74	0.04	-2.74	0.04
20	-2.64	-2.71	0.07	-2.58	-0.06
21	-2.46	-2.50	0.04	-2.45	-0.01

[a]Compounds in the test set.

calculated by the Gasteiger-Hückel method.

3D-QSAR Analysis.

Molecular Alignment. Molecular alignment is considered as a crucial step for 3D-QSAR study.[23] In order to develop possible accurate and reliable CoMFA and CoMSIA model, three different alignment rules were adopted. The first rule was ligand-based alignment (alignment I). During this process, the most potent compound **7** was chosen as template and the remaining compounds were aligned based on an atom-by-atom fitting principle. Figure 1(a) shows the common substructure chosen in the template, which is marked by asterisks. Figure 1(b) depicts the result of alignment I. The second rule was the receptor-based alignment (alignment II). In this approach, the bioactive conformation of each compound obtained from molecular docking were aligned automatically and imported directly into a molecular database for CoMFA and CoMSIA researches. The alignment result based on alignment II is shown in Figure 1(c). Alignment III was similar to alignment I, but all the molecular conformations aligned to compound **7** were gained from molecular docking. The resulted alignment model is described in Figure 1(d).

CoMFA and CoMSIA Field Calculations: To derive the CoMFA and CoMSIA fields, a 3D cubic lattice with grid spacing of 2.0 Å in all directions was created to encompass the aligned molecules. In CoMFA analysis, the steric and electrostatic fields were calculated by an sp^3 carbon probe atom with charge of +1.0 and van der Waals radius of 1.52 Å. To minimize the influence of noise, the fields generated
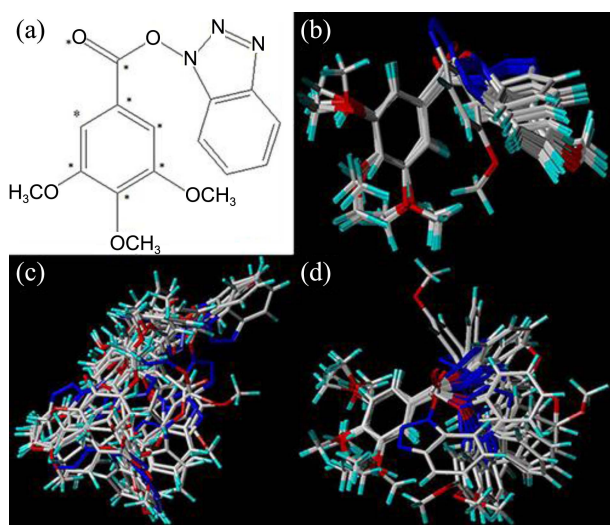
Figure 1. The alignments of compounds in the data set. (a) The chemical structure of template compound **7**, of which common substructure is marked by asterisks. (b-d) The superimpositions from the alignments from I, II, and III, respectively.

were scaled with default cut-off energy of 30 kcal/mol. In CoMSIA, a Gaussian-type function was used to evaluate the distance between the probe atom and the molecule atoms.[24] Besides steric and electrostatic fields, three other different fields are calculated: hydrophobic, hydrogen bond donor, and hydrogen bond acceptor. The default value of 0.3 was used as the attenuation factor.

3D-QSAR Model Generation: In 3D-QSAR, partial least squares (PLS) method[25] was adopted to analyze the training set, with the CoMFA/CoMSIA descriptors as independent variables and biological activity as the dependent variable. First, leave-one-out (LOO) cross-validation analysis with a minimum sigma (column filtering) of 2.0 kcal/mol was conducted to determine the optimum number of components (ONC) and cross-validation correlation coefficient (q^2). Second, a non-cross-validation analysis was performed using the ONC, which were determined by the first cross-validation stage, to generate a predictive 3D-QSAR model. The q^2 is a statistical parameter of the predictive ability of the model, and it is calculated by the following equation:

$$q^2 = 1 - \frac{\sum_{i=1}^{n}(Y_{predicted} - Y_{observed})^2}{\sum_{i=1}^{n}(Y_{observed} - Y_{mean})^2} \quad (1)$$

where n is the number of compounds, $Y_{predicted}$, $Y_{observed}$ and Y_{mean} are the predicted, observed and mean values of the target activity (pIC_{50}), respectively. The non-cross-validation correlation coefficient (r^2), the standard error of estimate (SEE), and F value were computed to evaluate the statistical significance of the non-cross-validation results.

3D-QSAR Model Validation: To further assess the robustness and statistical significance of the derived models, some internal validation strategies were performed. In addi-

tion to the LOO cross-validation, the leave-many-out (LMO) cross-validation using 2 groups (LMO_2) and 5 groups (LMO_5)[26] repeated 25 times was also performed to further assess the internal predictive ability. To measure the bias of the original calculation, bootstrap analysis[27] for 100 runs was conducted. To eliminate the possibility of chance correlation and ensure the robustness of 3D-QSAR models, Y-randomization[28] was performed for 10 times.

External validation is the most acceptable validation method to test the predictive ability of a QSAR model. The activities of the compounds in the test set, which were not used in the model generation, were predicted using the model generated from training set. A predicted r^2 ($r^2_{pred.}$) was then obtained according to:

$$r^2_{pred.} = 1 - \frac{PRESS}{SD} \quad (2)$$

where SD represents the sum of squared deviations between the experimental activities of the compounds in the test set and the average activity of the compounds in the training set, PRESS represents the sum of squared deviations between experimental and predicted activity values.

Molecular Docking. In order to identify the probable bioactive conformations and investigate the detailed binding modes between HDLP and benzotriazoles, molecular docking analysis was performed by the Surflex-dock module[29] in Sybyl 7.3 in this study. The crystal structure of HDLP was obtained from the RCSB Protein Data Bank (PDB code: 1C3R). Prior to docking, all cocrystallized ligands (Trichostatin A) and water molecules were removed and polar hydrogen atoms were added in standard geometry using the Biopolymer modulator. Then, the ligands were docked into the obtained binding site of HDLP with an empirical scoring function and a patented search engine in Surflex-Dock.

During the docking process, automatic-based approach was applied to generate protomol. In this process, two parameters, protomol_bloat and protomol_threshold, which determine the volume and extent of the protomol, were specified default values of 0 and 0.50, respectively. With other parameters setting default, all of the compounds were docked into the binding pocket, and top 10 options of binding conformation ranked by total scores were obtained for each compound. The highest-scored conformation based on the Surflex-Dock scoring function for each ligand, was selected as the most likely bioactive conformation and used for receptor-based CoMFA and CoMSIA researches.[30]

Before docking analysis, in order to straightforward evaluate the accuracy of molecular docking, the cocrystallized ligand Trichostatin A was redock into the binding pocket of receptor. The docking method is rational if the root mean square deviation (RMSD) value between the basic skeleton of the best-scored and the crystal conformation is less than 2.0 Å.[31]

Results and Discussion

3D-QSAR Statistical Results. The statistic results of the

Table 3. Statistical results of CoMFA and CoMSIA models

	Alignment I		Alignment II		Alignment III	
	CoMFA	CoMSIA	CoMFA	CoMSIA	CoMFA	CoMSIA
PLS statistics						
ONC	3	5	2	3	6	6
q^2	0.647	0.685	-0.089	-0.257	0.213	0.033
r^2	0.968	0.928	0.831	0.930	0.999	0.998
SEE	0.143	0.232	0.316	0.212	0.025	0.039
F	131.544	25.511	34.380	57.257	2129.273	926.977
Field contribution%[a]						
S	62.7	18.2	42.0	19.0	48.2	13.2
E	37.3	35.3	58.0	37.1	51.8	34.4
H	NA	17.1	NA	23.3	NA	28.0
D	NA	14.7	NA	10.8	NA	15.8
A	NA	14.7	NA	9.8	NA	8.5

[a]Abbreviations: S: steric field, E: electrostatic field. H: hydrophobic field. D: hydrogen bond donor field, A: hydrogen bond accept field, and NA, not applicable.

CoMFA and CoMSIA models using three different alignment rules are summarized in Table 3. Since the CoMFA and CoMSIA models are alignment sensitive, different alignment rules may lead to the differences of quality and predictive ability for the models. As shown in Table 3, both CoMFA and CoMSIA models based on alignment I exhibit better statistic results than those obtained from alignment II and III. Thus, the alignment I models were focused on in the following discussion. In the alignment I models, the cross-validation analysis of CoMFA and CoMSIA yielded a q^2 of 0.647 and 0.685, respectively. The non-cross-validation analysis sequentially gave an r^2 of 0.968 (with SEE of 0.143) and 0.928 (with SEE of 0.232), respectively. For the CoMFA model, the steric contribution was nearly twice of the electrostatic contribution. For the CoMSIA model, the introduction of hydrophobic interaction, hydrogen bond donor, and hydrogen bond acceptor reduced the contribution of steric interaction.

In addition to the LOO cross-validation, based on two groups and five groups, the LMO cross-validation was also carried out for 25 times. The mean q^2 of LMO_2 and LMO_5 for CoMFA were 0.576 and 0.643, respectively. For CoMSIA, the corresponding mean q^2 values were 0.576 and 0.659, respectively. The bootstrap validation for 100 runs was performed. The r^2_{bs} and SEE_{bs} values were 0.972 and 0.129 for CoMFA as well as 0.978 and 0.134 for CoMSIA, respectively. These results suggested that the models were robustness and have high internal predictive ability.

To further eliminate the possibility of chance correlation, the Y vector (pIC$_{50}$ values) were randomized for 10 times. As a result, the q^2 and r^2 values of CoMFA were in the ranges of −0.387 to 0.251 and 0.256 to 0.648, respectively. For CoMSIA, the q^2 and r^2 obtained were in the ranges of −0.263 to 0.179 and 0.164 to 0.613, respectively. The low values of q^2 and r^2 indicated that the results from both the CoMFA and CoMSIA models were not due to chance correlations.

External validation was also performed to further assess the external predictive ability of the CoMFA and CoMSIA

models. This validation was performed using an external test set including 4 compounds not included in the development of the 3D-QSAR model. The corresponding r^2_{pred} were 0.687 and 0.555 for CoMFA and CoMSIA models, respectively. The predicted pIC$_{50}$ values for the training set and the test set are listed in Table 2, and the correlations between predicted
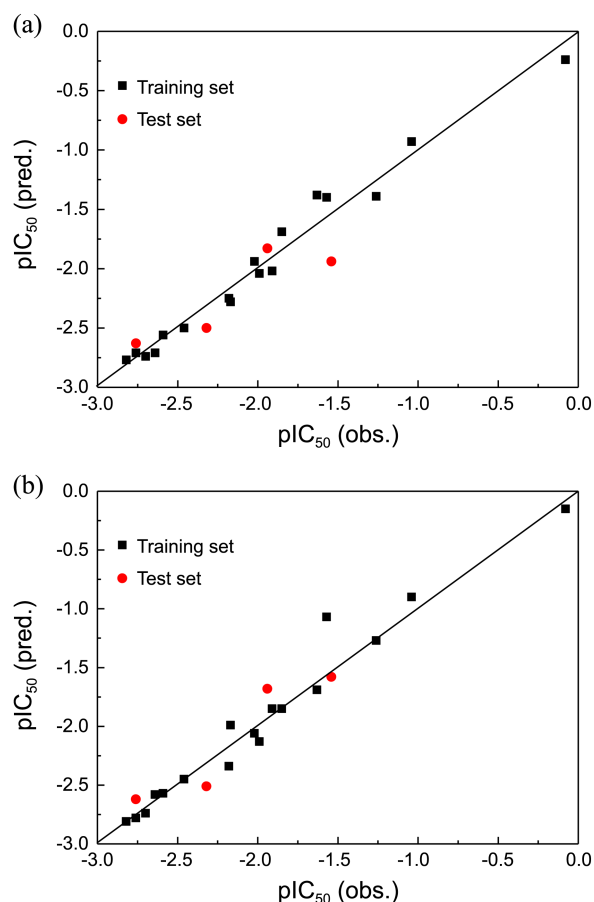
Figure 2. Plots of predicted pIC$_{50}$ values *versus* the corresponding observed values for compounds in the training and test set. (a) CoFMA model, and (b) CoMSIA model.
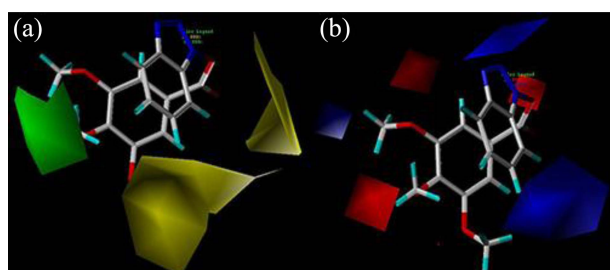
Figure 3. CoMFA contour maps with the combination of compound **7**. (a) Steric contour map, and (b) Electrostatic contour map.

and observed pIC_{50} values are shown in Figure 2. The predicted pIC_{50} values were in good consistency with the observed values, indicating the strong predictive ability of the obtained model,

3D-QSAR Contour Maps. One of the most attractive features of CoMFA and CoMSIA is visualization of the results. The visualization of the 3D-QSAR model was represented by field contour maps, where the coefficients were generated using the field type "Stdev*Coeff" (the standard deviation and the coefficient) with default values of 80% favored and 20% disfavored contributions. To aid in visualization, the most potent compound **7** is shown in the contour maps.

CoMFA Contour Maps: The steric and electrostatic field contour maps from the CoMFA model are shown in Figure 3. In the CoMFA steric contour (Figure 3(a)), the steric interactions are represented by green and yellow contours, where sterically bulky substituents close to the green regions would increase the activity but they are unfavorable when near the yellow regions. A large green contour was found cover the 4-position of benzene ring, suggesting that compounds with bulkier groups at the position should be more active than those with no or smaller groups. This was in line with the higher activity of compound **19** ($pIC_{50} = -2.70$), which have a bulky group ($-OCH_3$), than the activities of compound **16** ($pIC_{50} = -2.76$) and compound **15** ($pIC_{50} = -2.82$), which have the $-OH$ group and H atom at this position, respectively. In addition, a large yellow contour map was appeared around the 3-position of the benzotriazole ring, indicating that its preference for the steric moderate and less crowded substituents here. This may explained why the compounds **1-7** with H atom at 3-position of the benzotriazole ring exhibited higher activities than compounds 8-14, which have the substituents $-OCH_3$, excepted compounds **6** and **13** showed similar activities. Besides, a large region of yellow contour

was seen near the carbonyl, which denoted that add bulk substituents to this position may decrease the activity.

The electrostatic contour map is depicted in Figure 3(b), where the blue regions represent the electropositive groups near these regions is favorable to the activity and the red regions indicate that the electronegative groups close to these regions may increase the activity. A mid-sized blue region was found near to 2-position of benzotriazole ring, demonstrated that a relatively more electropositive group at this position are favorable for enhancing activity. The large blue contour was located at the 6-position of benzotriazole ring, implying an electropositive substituent at this position would increase activity. This may explain why the pIC_{50} of compounds **4** and **7** was almost 4.5 and 10 times greater than that of compounds **11** and **14**, respectively. Moreover, there were both blue and red contours around the 5-position of benzene ring. These observations indicated that a careful selection of groups is required.[32] Besides, a mid-sized red contour was found near the 4-position of benzene ring, suggesting that the presence of electronegative groups herein was helpful for the increase of activity. This was why compound **21** with $-OCH_3$ at this position present larger potency than compound **20** with H atom. And it was the same case for the different activities between compounds **4** and **3**. In addition, the small red region located on 1-position of benzotriazole ring demonstrated that electronegative substituents were desirable at this position for the improvement of activity.

CoMSIA Contour Maps: The CoMSIA steric, electrostatic, hydrophobic, hydrogen bond donor, and hydrogen bond acceptor field contour maps are shown in Figure 4. The steric and electrostatic field contour maps of CoMSIA were found to be similar to those of CoMFA except for several slight differences. Therefore only the hydrophobic, hydrogen bond donor, and hydrogen bond acceptor field contour maps were discussed here.

In the CoMSIA hydrophobic contour map (Figure 4(c)), the white contour is hydrophilic-favorable, while the yellow contour is hydrophobic-favorable. As can be seen, a mid-sized white contour was surrounded with the 4-position of benzene ring, implying that hydrophilic groups at this position may be beneficial to the activity. This may explain why compounds **2** and **18** showed higher activities than compounds **1** and **17**, respectively. However, it can be noted that above the white contour there was also a yellow-colored contour. Thus a careful selection of group at this position
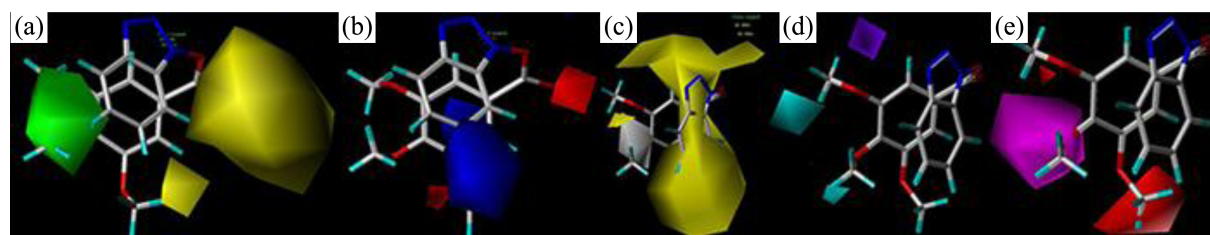
Figure 4. CoMSIA contour maps with the combination of compound **7**. (a) Steric contour map, (b) Electrostatic contour map, (c) hydrophobic contour map, (d) hydrogen bond donor contour map, and (e) hydrogen bond donor accept contour map.

was necessary. This could be illustrated by the example that compound **21** exhibited higher potency than compound **20**. The experimental result that compound **5** had higher ability than compound **2** was also such a case. In addition, it can be recognized that the benzotriazole ring had been encompassed by a large yellow contour. Therefore it can be reasonably assumed that the benzotriazole ring core with hydrophobic substituent could increase activity.

The hydrogen bond donor and acceptor contour maps are depicted in Figure 4(d) and Figure 4(e). The cyan and purple contours represent regions where hydrogen bond donor group would be favorable and unfavorable to the activity, respectively. While the favored hydrogen bond acceptor regions are shown in magenta and disfavored regions in red, respectively. The small cyan contour near 4-position of benzene ring demonstrated that add hydrogen bond donor group at this position may increase the potency. This result could be supported by the comparison of compounds **7** and **6**, as well as compounds **21** and **19**. However, a large magenta contour was also found located at this position, indicating that a hydrogen bond acceptor group at this position may improve the activity. The appearance of both hydrogen bond donor and acceptor contours at the same position revealed that the group at this position may take part in the formation of hydrogen bond with receptor and influence the potential activity. Moreover, near 5-position of benzene ring, a cyan region and a purple region were located. So at this position, a careful selection of groups with electron-withdrawing or electron-donating ability was required. The large red region surrounded the 3-position of benzene ring depicted its disfavor for the hydrogen bond acceptor group. This was why compounds **4** and **16** (with low hydrogen bond acceptor group) exhibited larger potency than their counterparts, compounds **5** and **15**, respectively.

Molecular Docking. The control re-docking using the parameters specified in Surflex-Dock produced a conformation of Trichostatin A with a RMSD of 0.83 Å from the crystal structure. Then, all compounds in the data set were docked into the active site of HDLP. In order to illustrate the interaction mechanism between the ligand and the protein, the attention has been focused on ligand-protein interactions of the most active compound **7** and the least active compound **15**. The binding modes of compounds **7** and **15** are shown in Figure 5.

As illustrated in Figure 5(a), compound **7** was anchored in the binding site *via* hydrophobic and hydrogen bond interactions. The benzene ring was accommodated into the basically hydrophobic pocket that was composed of residues Try12, Gly13, Try17, Val28, and Ala98. The benzotriazole ring formed hydrophobic contacts with another hydrophobic center formed among Pro126, Ala127, Gly128, Met130, Phe141, and Gly293. This observation reached good agreement with the result of CoMSIA hydrophobic contour map. In addition, the aromatic ring of Tyr12 was capable of making π-π interactions with aromatic ring of compound **7**, which helped to control the conformation of the ligand at the binding pocket. Besides the important effect of hydrophobic
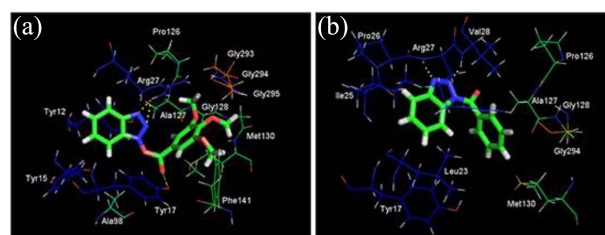
Figure 5. The binding modes between ligands and receptor. (a) Compound **7**, and (b) Compound **15**.

interactions, three hydrogen bonds playing crucial roles in anchoring the ligand at the binding pocket were also observed. The –NH of residue Arg27 formed two hydrogen bonds with two nitrogen atoms at 2-position and 3-position of the benzotriazole ring, with the bond angles of 120.8° and 145.5°, and the bond lengths of 2.5 Å and 1.9 Å, respectively. Additional, a hydrogen bond was also formed between the Try17 and carbonyl of the ligand with the bond angle and length of 166.4° and 3.1 Å, respectively.

The probable binding mode of compound **15** is displayed in Figure 5(b). It can be seen that many residues (Ala127, Gly128, Met130, Gly293, and Gly294) were capable of forming hydrophobic interactions that could potently control the conformation of benzene ring. Furthermore, the benzotriazole ring of compound **15** may form hydrophobic interactions with Tyr17, Lys24, Ile25, Pro26, and Phe141 of the receptor. In addition, altogether two hydrogen bonds were observed to stabilize the conformation of compound **15**. Specifically, the nitrogen atom at 2-position of the benzotriazole ring participated into a hydrogen bond with the backbone NH group of residue Arg27 with the bond angle of 146.1° and the bond length of 3.1 Å. Besides, another important hydrogen bond was observed between nitrogen atom at 3-position of the benzotriazole ring and Val28 with an angle of 130.6° and a length of 2.9 Å.

The above analysis showed that hydrophobic interactions and hydrogen bonds played an important role in the binding of ligand to receptor. Comparing compound **7** with compound **15**, the hydrophobic interactions were different in the binding pocket, and compound **15** could not form hydrogen bond with Try17 to fix its place. These differences in the ligand-receptor binding modes were mainly responsible for the different activities of the two compounds.

Conclusion

In this study, 3D-QSAR and molecular docking analysis were applied to characterize a set of recently synthesized antiproliferative agents. The optimal ligand-based CoMFA and CoMSIA models were generated, and both models exhibited good statistical significances and predictive abilities according to the statistical parameters, such as q^2, r^2, and r^2_{pred}, from both internal and external validations. The resulting contour maps derived from the CoMFA and CoMSIA models visualized the regions of structural features influence the antiproliferative activities of benzotriazoles. Furthermore,

the docking studies indicated that the hydrophobic interactions with residues in the hydrophobic pocket and hydrogen bonds with residues such as Try17, Arg27, and Val28 primarily resulted in the difference for activities. These results would be helpful in the rational design of novel benzotriazoles with more potent antiproliferative activities.

References

1. Jemal, A.; Bray, F.; Center, M. M.; Ferlay, J.; Ward, E.; Forman, D. *Ca: A Cancer J. Clin.* **2011**, *61*, 69.
2. Ma, X.; Xiang, G. Y.; Yap, C. W.; Chui, W. K. *Bioorg. Med. Chem. Lett.* **2012**, *22*, 3194.
3. Gomez-Perez, V.; McSorley, T.; Too, W. C. S.; Konrad, M.; Campos, J. M. *Chemmedchem* **2012**, *7*, 663.
4. Markovic, V.; Eric, S.; Stanojkovic, T.; Gligorijevic, N.; Arandelovic, S.; Todorovic, N.; Trifunovic, S.; Manojlovic, N.; Jelic, R.; Joksovic, M. D. *Bioorg. Med. Chem. Lett.* **2011**, *21*, 4416.
5. Drakulic, B. J.; Stanojkovic, T. P.; Zizak, Z. S.; Dabovic, M. M.. *Eur. J. Med. Chem.* **2011**, *46*, 3265.
6. Liu, J.; Li, Y.; Zhang, H. X.; Zhang, S. W.; Yang, L. *J. Mol. Model.* **2012**, *18*, 991.
7. Taft, C. A.; Da Silva, V. B.; Da Silva, C. *J. Pharm. Sci.* **2008**, *97*, 1089.
8. Phosrithong, N.; Samee, W.; Ungwitayatorn, J. *Med. Chem. Res.* **2012**, *21*, 559.
9. Madhavan, T.; Kothandan, G.; Gadhe, C. G.; Cho, S. J. *Med. Chem. Res.* **2012**, *21*, 681.
10. Ghasemi, J. B.; Shiri, F. *Med. Chem. Res.* **2012**, *21*, 2788.
11. Xu, Y. Y.; Zhang, L.; Li, M. Y.; Xu, W. F.; Fang, H.; Shang, L. Q. *Med. Chem. Res.* **2012**, *21*, 1000.
12. Islam, M. A.; Pal, R.; Hossain, T.; Mukherjee, A.; Saha, A. *Med. Chem. Res.* **2012**, *21*, 2652.
13. Li, X.L.; Ye, L.; Wang, X.X.; Wang, X. Z.; Liu, H. L.; Zhu, Y. L.; Yu, H. X. *Toxicol. Appl. Pharm.* **2012**, *265*, 300.
14. Wang, X. X.; Li, X. L.; Shi, W.; Wei, S.; Giesy, J. P.; Yu, H. X. *Ecotox. Environ. Safe*. **2013**, *89*, 143.
15. Handratta, V. D.; Vasaitis, T. S.; Njar, V. C. O.; Gediya, L. K.; Kataria, R.; Chopra, P. *J. Med. Chem.* **2005**, *48*, 2972.
16. Saczewski, F.; Dziemidowicz-Borys, E.; Bednarski, P. J.; Gdaniec, M. *Archiv. Der. Pharmazie*. **2007**, *340*, 333.
17. Katritzky, A. R.; Yoshioka, M.; Narindoshvili, T.; Chung, A.; Khashab, N. M. *Chem. Biol. Drug. Des.* **2008**, *72*, 182.
18. Rajic, Z.; Butula, I.; Zorc, B.; Pavelic, S. K.; Hock, K.; Pavelic, K. *Chem. Biol. Drug. Des.* **2009**, *73*, 328.
19. Fu, J.; Yang, Y.; Zhang, X. W.; Mao, W. J.; Zhang, Z. M.; Zhu, H. L. *Bioorg. Med. Chem.* **2010**, *18*, 8457.
20. Grunstein, M. *Nature* **1997**, *389*, 349.
21. Mai, A.; Massa, S.; Ragno, R.; Cerbara, I.; Jesacher, F.; Loidl, P.; Brosch, G. *J. Med. Chem.* **2003**, *46*, 512.
22. Clark, M.; Cramer, R. D.; Vanopdenbosch, N. *J. Comput. Chem.* **1989**, *10*, 982.
23. Li, X. L.; Ye, L.; Wang, X. X.; Wang, X. Z.; Wang, X. Z.; Liu, H. L.; Yu, H. X. *Sci. Total Environ.* **2012**, 441, 230.
24. Zheng, J. X.; Xiao, G. K.; Guo, J. L.; Rao, L. Y.; Chao, W.; Zhang, K.; Sun, P. H. *J. Mol. Model.* **2011**, *17*, 2113.
25. Wold, S.; Ruhe. A.; Wold, H.; Dunn, W. J. *SIAM J. Sci. Stat. Comp.* **1984**, *5*, 735.
26. Yang, W. H.; Shen, S.; Mu, L.; Yu, H. X. *Environ. Toxicol. Chem.* **2011**, *30*, 2431.
27. Aparoy, P.; Suresh, G. K.; Reddy, K. K.; Reddanna, P. *Bioorg. Med. Chem. Lett.* **2011**, *21*, 456.
28. da Cunha, E. F. F.; Mancini, D. T.; Ramalho, T. C. *Med. Chem. Res.* **2012**, *21*, 590.
29. Jain, A. N. *J. Comput. Aided Mol. Des.* **2007**, *21*, 281.
30. Wu, X. Y.; Wu, S. G.; Chen, W. H. *J. Mol. Model.* **2012**, *18*, 1207.
31. Shen, X. L.; Takimoto-Kamimura, M.; Wei, J.; Gao, Q. Z. *J. Mol. Model.* **2012**, *18*, 203.
32. Hao, M.; Li, Y.; Wang, Y.; Yan, Y.; Zhang, S. *J. Chem. Inf. Model.* **2011**, *51*, 2560.